Showcasing research on biocomposites from Professor Chang Geun Yoo's laboratory, Department of Chemical Engineering, State University of New York College of Environmental Science and Forestry, United States.

Effects of chemical composition and physicochemical properties of poplar biomass on the performance of 3D printed poplar-reinforced PLA materials

This research demonstrated how chemical pretreatments of poplar biomass impact the final performance of 3D-printed biocomposites. By systematically correlating biomass characteristics with composite mechanical and thermal behaviour, the key structure-property-performance relationships were revealed. This study highlighted both the potential of untreated wood as a sustainable filler and the value of tailored pretreatments for tuning composite performance, providing a foundation for engineering renewable, high-performance materials for sustainable additive manufacturing.

Image reproduced by permission of Chang Geun Yoo from *RSC Sustainability*, 2025, **3**, 4478.

Image created with Microsoft Copilot.

As featured in:

See Arthur J. Ragauskas, Chang Geun Yoo *et al.*, *RSC Sustainability*, 2025, **3**, 4478.

ROYAL SOCIETY OF CHEMISTRY

rsc.li/rscsus

Registered charity number: 207890

RSC Sustainability

ROYAL SOCIETY OF CHEMISTRY

PAPER

View Article Online
View Journal | View Issue

Check for updates

Cite this: *RSC Sustainability*, 2025, **3**, 4478

Effects of chemical composition and physicochemical properties of poplar biomass on the performance of 3D printed poplar-reinforced PLA materials

Anqi Ji, [ab] Samarthya Bhagia, [c] Nara Han, [a] Kwang Ho Kim, [d] Gyu Leem, [e] Nidia C. Gallego, [f] Shuyang Zhang, [g] Kai Li, [h] Soydan Ozcan, [i] Arthur J. Ragauskas *[cgjk] and Chang Geun Yoo *[a]

Lignocellulosic biomass has been well-acknowledged as a filler for making 3D printed composites. The technical performances of composites were influenced by the characteristics of the components. The correlations between poplar biomass properties and the mechanical and thermal performances of the 3D printed poplar-plastic composites were investigated. The characteristics of poplar were modified by different pretreatment methods, including using hot water, dilute acid, and organic solvent (organosolv), and each treated poplar biomass was applied as a filler in a polylactic acid (PLA) polymer matrix to produce eco-friendly materials. These solvent pretreatments increased the hydrophobicity and surface area of poplar. Organosolv treated poplar showed the highest cellulose content and significantly increased Young's modulus of its biocomposites. Principal component analysis revealed that the specific surface area and water contact angle of biomass contributed to the thermal stability of biocomposites. Additionally, the degree of polymerization of cellulose and xylan content within the biomass correlated with the biocomposites' break stress. Notably, the crystallinity of biocomposites impacted the modulus of these materials. The reported relationships between biomass characteristics and 3D printed composite behaviors provide guidance for optimizing biomass processing in biocomposite applications.

Received 6th May 2025
Accepted 17th August 2025

DOI: 10.1039/d5su00327j

rsc.li/rscsus

Open Access Article. Published on 03 9 2025. Downloaded on 2026-04-26 3:20:06.
This article is licensed under a Creative Commons Attribution 3.0 Unported Licence.

Sustainability spotlight

The heavy use of petroleum-based plastics has led to a global energy and environmental crisis. To address this problem, researchers shifted towards green, renewable, and environmentally friendly biopolymers and their composites. Lignocellulosic biomass has been applied to reinforce a variety of bioplastics. However, the complexity and heterogeneity of biomass limit their composite applications. This study investigates how the physicochemical properties of woody biomass, modified through various processing methods, affect the performance of 3D printed wood-reinforced PLA composites. Our findings highlight the relationship between biomass characteristics and 3D printed composite behavior, offering guidance for optimizing biomass processing in biocomposite applications. By demonstrating the potential to replace conventional plastics with biomass-based composites in 3D printing, the results in this study support the advancement of sustainable manufacturing practices in line with the United Nations Sustainable Development Goal 9: Industry, Innovation, and Infrastructure.

[a]*Department of Chemical Engineering, State University of New York, College of Environmental Science and Forestry, Syracuse, NY 13210, USA. E-mail: cyoo05@esf.edu*
[b]*Department of Chemical Engineering, Howard University, Washington, DC 20059, USA*
[c]*Biosciences Division, Oak Ridge National Laboratory, TN 37831, USA*
[d]*Department of Wood Science, University of British Columbia, Vancouver, BC, V6T 1Z4, Canada*
[e]*Department of Chemistry, State University of New York, College of Environmental Science and Forestry, Syracuse, NY 13210, USA*
[f]*Chemical Sciences Division, Oak Ridge National Laboratory, Oak Ridge, TN, 37830, USA*
[g]*Department of Chemical and Biomolecular Engineering, University of Tennessee Knoxville, Knoxville, TN 37996, USA. E-mail: aragausk@utk.edu*
[h]*Buildings and Transportation Science Division, Oak Ridge National Laboratory, Oak Ridge, TN 37831, USA*
[i]*Manufacturing Sciences Division, Oak Ridge National Laboratory, Oak Ridge, TN, 37830, USA*
[j]*Center for Bioenergy Innovation, University of Tennessee-Oak Ridge National Laboratory Joint Institute for Biological Science, Knoxville, TN 37831, USA*
[k]*Department of Forestry, Wildlife and Fisheries, Center for Renewable Carbon, University of Tennessee Knoxville, Institute of Agriculture, Knoxville, TN 37996, USA*

© 2025 The Author(s). Published by the Royal Society of Chemistry

Open Access Article. Published on 03 9 2025. Downloaded on 2026-04-26 3:20:06.
This article is licensed under a Creative Commons Attribution 3.0 Unported Licence.

1 Introduction

Three-dimensional (3D) printing is a manufacturing technique that is defined as the process of joining materials layer upon layer to make objects from 3D-model designs.[1] It is a promising material-efficient additive manufacturing technology that allows the production of complex shapes. Several 3D printing methods, such as selective laser sintering (SLS), stereolithography (SLA), fused deposition modeling (FDM), and inkjet printing, have been applied for printing metals, ceramics, polymers, and concrete. Among these technologies, FDM is one of the most common additive manufacturing methods because of its low cost, high printing speed and simplicity, as it uses easy-to-use filaments. FDM can also be operated without complex computer knowledge.[2,3]

Commercially available thermoplastic materials such as acrylonitrile butadiene styrene (ABS), polypropylene (PP), polycarbonate (PC), polylactic acid (PLA), and polyetherimide (PEI) are commonly used in the FDM process. Among them, PLA is a renewable and biocompostable thermoplastic. Its monomer, lactic acid, is a biomass-derived platform chemical obtained through fermentation of carbohydrates. Due to the depletion of fossil fuels and the increasing environmental issues, lignocellulosic biomass has been a well-acknowledged alternative resource in many applications, such as bio-based fuels, chemicals, and materials.

In recent years, researchers have focused on biomass applications *via* 3D printing technology.[4] Previous studies reported that the addition of wood to plastic polymers increased their stiffness and bending properties.[5,6] Incorporating biomass as a reinforcing agent in biocomposite materials offers a promising strategy for reducing the environmental impact of 3D printed products. For example, Oh *et al.* demonstrated that even unconventional food-derived biomass, such as recycled tempura powder debris, can be successfully incorporated into biodegradable polymers for 3D printing, supporting the broader vision of sustainable additive manufacturing through biomass utilization.[7] Biomass is typically degraded more rapidly compared to the current plastic resins; thus, its addition shortens the degradation time of end-of-life products, leading to sustainable waste management practices.[8] However, the relatively low compatibility between biomass and typical commercial plastic resins often results in insufficient mechanical performance.[9] Additionally, the complexity and variability of biomass structure and composition, along with its physicochemical properties such as infusibility and insolubility in common solvents, limit its use in 3D printing.[10]

In recent years, significant efforts have been made to incorporate wood into PLA to fabricate sustainable and compostable composites with enhanced mechanical and thermal performance. However, most studies have been conducted with a single pretreatment method or randomly selected feedstock, which are not directly comparable to explain how various chemical or physical treatments impact both biomass properties and composite performance. In this study, to elucidate the impacts of biomass characteristics such as chemical composition, surface properties, hydrophobicity, and structural properties on the printed biocomposite materials, three chemical modification methods: liquid hot water (LHW),[11] dilute acid (DA),[12] and organosolv[13,14] pretreatments were applied to modify the biomass. Such a modification has not been carried out on biomass for the purpose of manufacturing 3D printed composites. Previous studies have shown that both LHW and DA selectively removed hygroscopic hemicellulose and increased the surface area, while organosolv pretreatment effectively removed amorphous components such as hemicellulose and lignin. The treated poplar was then used as a reinforcing filler in a PLA matrix, followed by extrusion and fabrication of 3D printed specimens *via* the FDM method. Also, we applied principal component analysis (PCA) to correlate these biomass characteristics with the mechanical and thermal properties of the resulting PLA composites. This multivariate statistical approach enables a more comprehensive understanding of structure–property–performance relationships, which have not been extensively explored in previous PLA/wood composite studies.

2 Materials and methods

2.1. Materials

Poplar was provided by Oak Ridge National Laboratory. The air-dried poplar chips (moisture content: 3.78%) were Wiley-milled to a 30-mesh and kept in a sealed plastic bag prior to the chemical modification and characterization. Sulfuric acid (72%), ethanol (100%), and dioxane (99%) were purchased from RICCA, Pharmco, and J. T. Baker, respectively. Polylactic acid (4043D, Ingeo Biopolymer) was procured from Natureworks LLC (Minnetonka, MN).

2.2. Thermochemical modification of poplar biomass

The milled poplar was treated by three thermochemical methods according to the literature (LHW,[11] DA,[12] and organosolv[13,14]). In brief, LHW pretreatment was conducted with deionized water at 200 °C for 20 min, and DA pretreatment was performed with 0.5% (w/w) H_2SO_4 at 160 °C for 10 min. Organosolv pretreatment was conducted with 1.25% (w/w) H_2SO_4 in 50% (v/v) ethanol at 180 °C for 1 h. The treated biomass was air-dried overnight and placed in a 105 °C oven for 8 h to remove the moisture. The untreated biomass and treated biomass were then ball-milled with two stainless-steel jars after nitrogen purging in a cold room (4 °C) for 6 h with a 30 min interval every hour.

2.3. Filament manufacturing and specimen 3D printing of PLA and poplar biomass

The overall process flow, including filament manufacturing and specimen FDM 3D printing, is illustrated in Fig. 1. In brief, ball-milled poplar (untreated and treated) and 2 mm knife-milled PLA were mixed at a 2 : 8 (w/w) ratio at room temperature. The well-mixed sample was kept in a vacuum oven at 80 °C for 8 h in order to remove moisture. A filament extruder (Filabot EX2, Filabot, Barre, VT) equipped with an air-path and spooler and

Open Access Article. Published on 03 9 2025. Downloaded on 2026-04-26 3:20:06.
This article is licensed under a Creative Commons Attribution 3.0 Unported Licence.

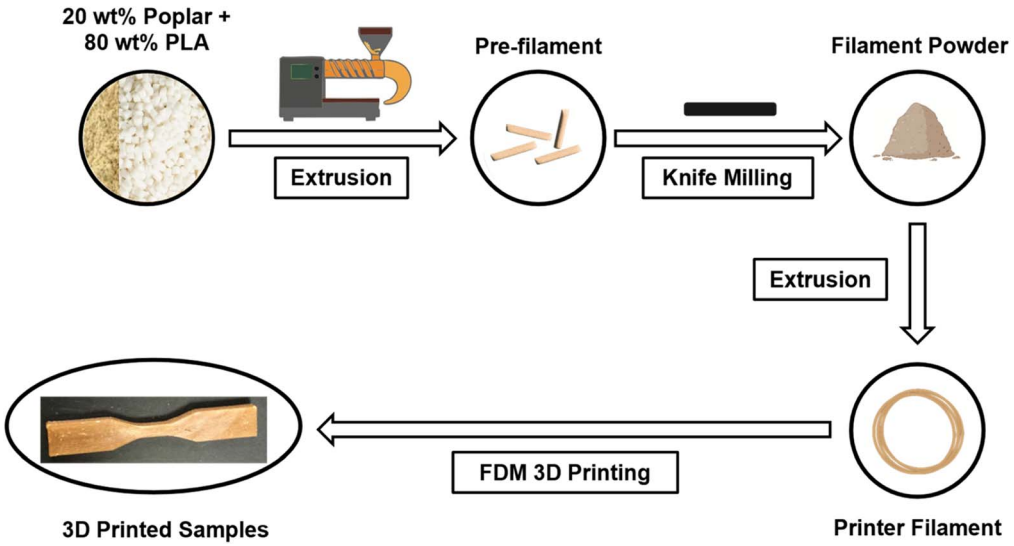

Fig. 1 Schematic diagram of the additive manufacturing process for producing PLA/poplar composites.

Lulzbot TAZ Workhorse 3D printer with a 0.5 mm SE Tool Head (FAME 3D, Fargo, ND) were used for filament formation and 3D printing. A Filabot EX2 single-screw extruder (length/diameter ratio of 12, 1.5875 cm screw diameter, 1.27 pitch, compression ratio of 2.5 : 1) was used to extrude the PLA/biomass filaments at 210 °C. Pure 2 mm knife-milled PLA was extruded to clean the extruder before starting each different extrusion run. After cleaning, the PLA/poplar mixture was loaded into the loading chute. The filament was then manually guided with no applied force and fan cooling. The filament produced by the first extrusion was then cut into ~1 cm long cylindrical pellets and knife-milled through a 2 mm screen (mini Wiley mill, Thomas Scientific). Milled powder was kept in a vacuum oven under the same conditions mentioned above. After 8 h of drying, the powder then underwent extrusion for the second time (the exact same way as the first extrusion) to produce a filament 1.6 mm in diameter for 3D printing. In order to avoid cross-contamination by the leftover from previous materials in the extruder barrel, a 1.5 m length of the initial filament was discarded.

The ASTM D638 Type V[15] 3D printed test specimens were designed in FreeCAD 0.18.4. G-code and produced in Cura 3.6.21 Lulzbot Edition for a Lulzbot TAZ Workhorse (0.5 mm SE tool head and glass/PEI print surface using only perimeter filling (0% infill), 0.3 mm layer height, 0.6 mm line width, 230 °C printing temperature, 20 mm s^{-1} print speed, constant 40 °C build plate temperature, 160 °C probe, soften and wipe temperature, 3 mm s^{-1} retraction speed, 1 mm retraction distance, 10 mm s^{-1} nozzle switch retraction speed, 100% flow rate, 175 mm s^{-1} travel speed, 15 mm s^{-1} skirt speed with 3 skirts, no print cooling, 35 °C part removal temperature). The printing layer was started at the corner of the tensile shape grip end and printed one sample at a time with each PLA/poplar sample in triplicate. All extrusion and 3D printing parameters, including extrusion temperature, printing temperature, bed temperature, printing speed, and layer height, were kept constant for all samples to ensure consistency in processing conditions. Further detailed manufacturing and 3D printing information is available in the previous study.[16]

2.4. Characterization of untreated and treated poplar biomass

Carbohydrate and lignin contents of biomass before and after pretreatment were measured according to the NREL standard procedure.[17] The hydrolysate from this procedure was used to analyze the carbohydrates and acid-soluble lignin. Carbohydrates were analyzed using a Young-Lin YL 9100 (Republic of Korea) high performance liquid chromatograph (HPLC), equipped with a Bio-Rad Aminex HPX-87H column and a refractive index detector, with 5 mM H_2SO_4 solution as the mobile phase at a constant flow rate of 0.6 mL min^{-1}. The acid-soluble lignin was measured by using a UV-vis spectrometer to obtain the absorbance at 240 nm wavelength and 25 L g^{-1} cm^{-1} was used as absorptivity of poplar for calculation.

Morphological properties of the biomass powder prior to ball-milling were analyzed using Scanning Electron Microscopy (SEM, JEOL-JSM-IT100LA). The sample was vacuum dried, mounted on an aluminum stub with carbon tape and sputter coating with gold/palladium prior to the analysis. The particle size of ball-milled biomass was measured by using a laser diffraction analyzer (Malvern S3500). Each sample was measured in triplicate, using a reflecting particle setting, irregular shape, and 20 s ultrasonication. The Brunauer–Emmett–Teller (BET) specific surface area of the ball-milled biomass was measured by using an Autosorb Station (Quantachrome Instruments) under vacuum drying at 40 °C and an outgas time of 12 h using nitrogen. Water contact angle measurements were carried out on a Drop Shape Analyzer (Kruss Scientific) by the sessile drop method at 23 °C.

Cellulose Degree of Polymerization (DP) of the biomass was measured by using a gel permeation chromatography (GPC) SECurity 1200 system. α-cellulose was isolated from the biomass based on the previous studies.[18] The weight-average degree of

© 2025 The Author(s). Published by the Royal Society of Chemistry

Open Access Article. Published on 03 9 2025. Downloaded on 2026-04-26 3:20:06.
This article is licensed under a Creative Commons Attribution 3.0 Unported Licence.

polymerization (DP_w) of cellulose and number-average degree of polymerization (DP_n) of cellulose were calculated from the measured cellulose molecular weight divided by the tricarbanilated cellulose repeating unit (519 g mol^{-1}). Fourier transform infrared spectroscopy (FTIR) analysis of untreated and treated poplar was conducted using a Spectrum One FTIR Spectrometer (PerkinElmer, Wellesley, MA, USA) equipped with a universal attenuated total reflection (ATR) accessory. The spectra were measured between 4000 cm^{-1} and 600 cm^{-1} with an average of 16 scans per sample. Thermogravimetric analysis (TGA) was performed from room temperature to 600 °C at 10 °C min^{-1} on a Q500 (TA Instruments) under an airflow of 40 mL min^{-1}. The onset temperature (decomposition temperature) of the sample was obtained from the curve based on ASTM E2550.[19]

2.5. Characterization of 3D printed specimens with PLA and poplar biomass

The tensile properties of 3D printed test specimens prepared as described above with PLA and poplar biomass were characterized by using a custom-built calibrated universal tensile tester. A load of 907.185 kg was used, and samples were secured onto an axial extensometer using rubber bands and then held using manual or hydraulic grips. Testing was conducted using a custom-made LabView program at 0.0254 mm s^{-1} strain rate, 21 °C and 20 data points per s. Ultimate tensile stress, break stress, and Young's modulus were measured as described in the previous study.[16]

The morphological properties of the 3D printed specimens were also characterized by SEM (JEOL-JSM-IT100LA) as described above. The water contact angle of the 3D printed specimens was investigated on a Drop Shape Analyzer (Kruss Scientific) as described above. Differential scanning calorimetry (DSC) analysis was performed in the heat/cool/heat mode on a Q200 instrument (TA Instruments). The testing specimens were ramped from 0 °C to 180 °C, followed by cooling to 0 °C and then heated up back to 180 °C at a ramping rate of 10 °C min^{-1}. The glass transition temperature (T_g), cold crystallization temperature (T_{cc}), and melting temperature (T_m) were determined from the second heating curve. The degree of crystallinity (X_c)[20] was calculated using eqn (1):

$$X_c = \frac{\Delta H_m - \Delta H_c}{w \times \Delta H_m^o} \quad (1)$$

where ΔH_m is the melting enthalpy of the sample, ΔH_c is the crystallization enthalpy of the sample, ΔH_m^o is the melting enthalpy for 100% crystalline PLA (taken as 93 J g^{-1}), and w is the weight fraction of PLA in the sample.

TGA was performed from room temperature to 600 °C at 10 °C min^{-1} on a Q500 (TA Instruments) under an airflow of 40 mL min^{-1}. The onset temperature (decomposition temperature) of the sample was obtained from the curve based on ASTM E2550.[19]

2.6. Principal component analysis

PCA was conducted using Origin 2021 to determine the main variables among the multivariate data regarding biomass properties and analyze the correlation among biomass composition, particle size, specific surface area, water contact angle, cellulose DP, and the performance of biocomposites. Parameter scores in the first two principal components were plotted to present the PCA results.[21]

3 Results and discussion

3.1. Characteristics of poplar biomass after different pretreatments

3.1.1. Changes in the chemical composition of poplar biomass. The composition of biomass, including cellulose, hemicellulose, and lignin, is important in determining the properties of biocomposite materials,[22] so it is an essential property to explain the technical performance of the biocomposites. In this study, three different pretreatments (LHW, DA, and organosolv) were applied to modify the chemical composition of poplar by removing or reducing the amorphous components like lignin and/or hemicelluloses. Fig. 2 presents the chemical composition (glucan, xylan and lignin) of untreated and treated poplar. For the untreated poplar, glucan content was the highest at 46.6%, followed by xylan at 14.2% and lignin at 24.7%. LHW treated poplar showed a higher glucan content at 63.6% and lignin content at 37.3% than untreated poplar, while a significant reduction of xylan content to 0.6% was observed. DA pretreatment resulted in a similar chemical composition to LHW (glucan content at 65.6%, xylan content at 0.2%, and lignin content at 33.0%). Organosolv treated poplar had the highest increase in glucan content at 78.8% but showed less lignin content (14.0%) and minimal xylan content (0.6%). The relative lignin contents were increased after LHW and DA pretreatments due to the selective removal of hemicellulose and the possible formation of pseudo-lignin during these pretreatment processes.[23,24] Both LHW and DA pretreatments selectively and effectively removed

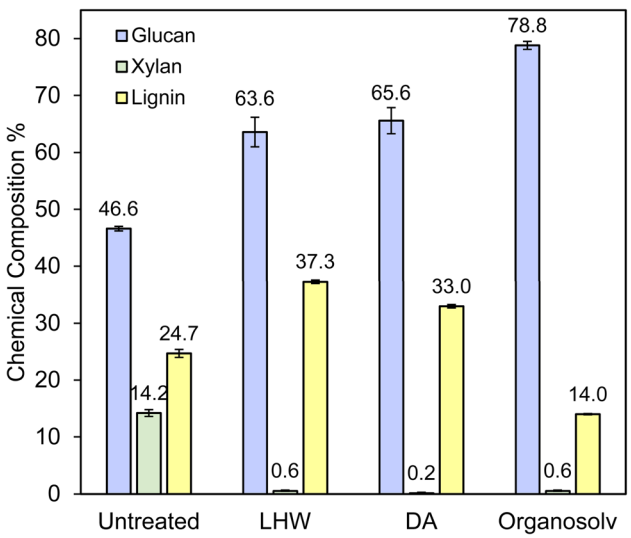

Fig. 2 Chemical composition (glucan, xylan, and lignin) of untreated and treated poplar.

Open Access Article. Published on 03 9 2025. Downloaded on 2026-04-26 3:20:06.
This article is licensed under a Creative Commons Attribution 3.0 Unported Licence.

hemicellulose (97.4% and 99.3% of xylan removal, respectively), while lignin content was not effectively extracted. However, organosolv pretreatment was effective in the removal of both hemicellulose and lignin from poplar and resulted in 98.1% xylan removal and 75.3% delignification. These results are consistent with the results in the previous studies.[11–13,25] The solid recoveries after LHW, DA, and organosolv pretreatments were 65.0%, 59.0%, and 43.6%, respectively.

3.1.2. Specific surface area and particle size of poplar biomass. Particle size is another crucial biomass characteristic that can affect the mechanical properties of polymeric composites.[5,26] Zhao *et al.* reported that the reinforcement with <180 μm of poplar biomass in the PLA-based composites led to better tensile properties than poplar samples with larger sizes.[5] The authors explained the improved mechanical properties with a higher surface area, surface porosity, and surface-to-volume ratio, which can be related to a better dispersion of poplar fiber with PLA. Specific surface area (SSA), which was obtained by BET analysis, can significantly impact the stiffness and strength of the composites.[27]

Table 1 shows the SSA and mean particle size of the ball-milled untreated, LHW treated, DA treated, and organosolv treated poplar. The untreated poplar had an SSA of 3.56 $m^2\ g^{-1}$ and a particle size of 39.49 μm. LHW pretreatment increased the SSA of poplar to 4.12 $m^2\ g^{-1}$ and decreased the particle size of biomass to 17.11 μm. A similar trend was observed by DA pretreatment, which resulted in a further increased SSA of 4.35 $m^2\ g^{-1}$ and a slightly smaller particle size of 16.72 μm. In contrast, the organosolv treated poplar showed an SSA of 3.90 $m^2\ g^{-1}$ and a larger particle size of 28.19 μm. The results indicated that all pretreatments decreased poplar particle size and increased SSA, which is consistent with the previous studies.[28–30] Compared to other treated poplars, organosolv treated poplar showed lower SSA and higher particle size mean. As mentioned previously, the ball-milling process was conducted after the pretreatment processes. The organosolv pretreatment led to a higher cellulose fraction, which has a more crystalline structure, possibly resulting in larger particle sizes in the ball-milling process. Compared to the amorphous components such as lignin and hemicellulose in poplar, which are more readily fractured, cellulose resists further size reduction during the ball-milling process due to its resilient nature.[31,32]

3.1.3. Water contact angle of poplar biomass. Due to the hygroscopicity of the biomass particles, stress transfer can be insufficient between the biomass powder and the hydrophobic polymer matrix.[33] Hence, different pretreatments were applied to improve the hydrophobicity of the poplar biomass, enhancing the compatibility between poplar particles and PLA. To evaluate the hydrophobicity of pure PLA, a water contact angle (WCA) measurement was conducted. The results revealed that the contact angle of the pure PLA 3D printed sample is 98° with a standard deviation of 3°, confirming its hydrophobic characteristic. The WCA for untreated, LHW, DA and organosolv treated poplar was 28 ± 3°, 50 ± 2°, 76 ± 3°, and 44 ± 2°, respectively. The contact angle of the water–biomass interface is related to lignin due to its hydrophobicity.[34] Therefore, the results indicated that these pretreatments increased the hydrophobicity of poplar biomass *via* chemical modifications. DA treated biomass showed the highest WCA compared to other treated/untreated poplar biomass because of the high lignin content and low hemicellulose content (Fig. 2). Also, hydrophobic pseudo-lignin formed during the DA pretreatment, confirmed by the increased lignin content, could increase the contact angle. Previous studies reported that pseudo-lignin, which was mainly comprised of carbonyl, carboxylic, and aromatic structures, was formed during dilute acid pretreatment of biomass.[35,36] According to the aforementioned chemical composition of untreated and treated poplar, the organosolv treated poplar biomass had the highest cellulose content among the samples and the lowest lignin content. The higher WCA of organosolv treated poplar compared to untreated poplar could be explained by residual lignin redistribution from bulk to the biomass surface which covered the cellulose fiber and increased its hydrophobicity.[37] For further verification of this hypothesis, SEM was performed to see the surface of organosolv treated poplar. As shown in Fig. 3, lignin (as indicated by the arrow) was observed and partially covered the organosolv treated fiber surface. This confirmed lignin redistribution onto the biomass surface during the pretreatment, leading to a higher water contact angle than that of untreated poplar, even though its lignin content was lower than that of the untreated one.

3.1.4. Chemical structure of biomass. The chemical structure of biomass can also be transformed by various pretreatments. To understand the structural changes of poplar *via* LHW, DA, and organosolv pretreatments, FTIR spectra of untreated and treated poplar samples were analyzed (Fig. 4). The broadband at around 3330 cm^{-1}, attributed to O–H stretching vibrations, and the peak near 2900 cm^{-1} (peak 1), corresponding to C–H stretching vibrations, remain relatively similar across all samples. The peak at 1730 cm^{-1} (peak 2), attributed to C=O stretching vibrations in hemicellulose and lignin, was reduced in treated biomass samples compared to that in untreated poplar, primarily due to the hemicellulose and/or lignin removals, as described in chemical composition results (Fig. 2). Among the pretreatments, the organosolv treated sample had the most significant reduction at peak 2, indicating high delignification and hemicellulose removal. The peak at 1610 cm^{-1} (peak 3), corresponding to asymmetric stretching of the carboxyl group of glucuronic acid in hemicellulose and C=O stretching in conjugated carbonyl of lignin, became more obvious in the spectra of LHW and DA treated biomass, which could be explained with the relatively increased

Table 1 BET specific surface area and particle size mean of the ball-milled untreated and treated poplar biomass

Sample	BET specific surface area ($m^2\ g^{-1}$)	Particle size mean (μm)
Untreated	3.56	39.49
LHW	4.12	17.11
DA	4.35	16.72
Organosolv	3.90	28.19

© 2025 The Author(s). Published by the Royal Society of Chemistry

Open Access Article. Published on 03 9 2025. Downloaded on 2026-04-26 3:20:06.
This article is licensed under a Creative Commons Attribution 3.0 Unported Licence.

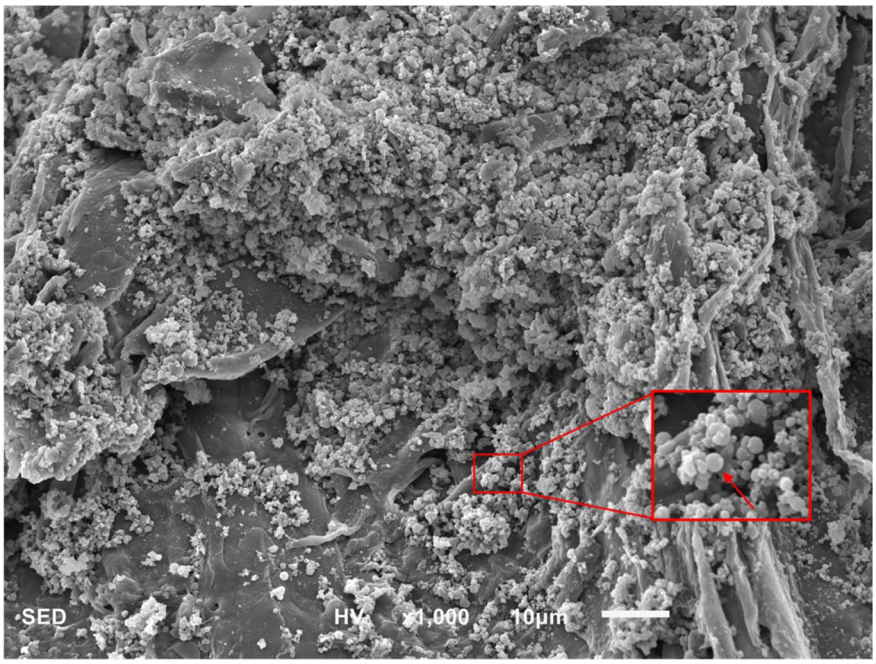

Fig. 3 SEM image of organosolv treated poplar, and the arrow indicated the spherical balls.

lignin content in the treated biomass by the removal of hemicellulose. In contrast, the spectrum of organosolv treated biomass showed a major decrease in this peak, indicating substantial lignin removal. Additional lignin-specific peaks at 1508 cm^{-1} (C=C–C aromatic ring stretching and vibration, peak 4) and 1457 cm^{-1} (C–H deformation in methyl and methylene, peak 5) were significantly lower in the spectrum of organosolv treated biomass, confirming its high delignification efficiency. Moreover, the peaks at 1160 cm^{-1} (peak 6) and 896 cm^{-1} (peak 7), attributed to C–O–C stretching in both cellulose and hemicellulose, became sharper and more intense with the organosolv treated biomass sample, reflecting an increased relative cellulose content and possibly enhanced crystallinity of poplar due to the removal of amorphous components like lignin and hemicellulose.[38]

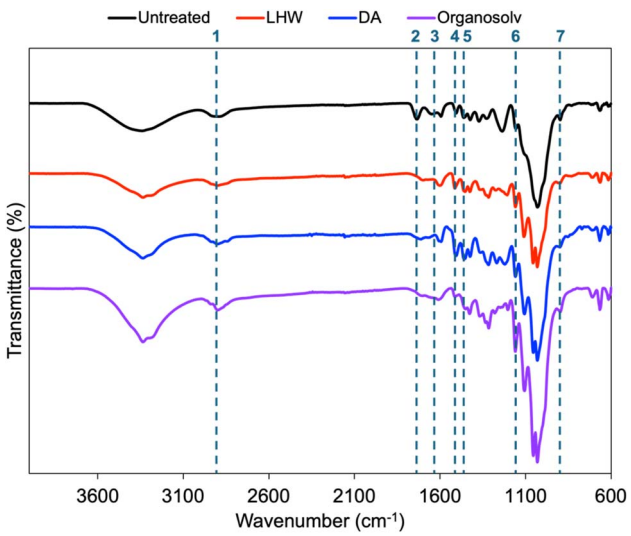

Fig. 4 FTIR spectra of untreated and treated poplar.

3.2. Performance of 3D printed wood-reinforced PLA biocomposites

3.2.1. Tensile properties of PLA/biomass biocomposites. The aforementioned poplar samples were blended with PLA, and then 3D printed to make composites by FDM. While PLA is a promising biocompostable polymer, it suffers from limitations such as brittleness, low thermal resistance, and poor crystallization behavior, which restrict its practical applications. We hypothesized that biomass pretreatments (*i.e.*, LHW, DA, and organosolv) could improve the compatibility of the biofiller to the PLA matrix by increasing the specific surface area and hydrophobicity. In addition, hydrogen bonding between the hydroxyl group (–OH) in biomass and the carbonyl group (–C=O) in PLA can enhance interfacial adhesion and load transfer.[39,40] The enhanced compatibility and interfacial reactions of biomass in the composites ensure a more uniform distribution of stress across the biocomposite, enhancing its mechanical properties. Thus, this strategy leverages the multifunctional role of biomass to overcome inherent weaknesses of PLA and broaden its utility in sustainable composite manufacturing.

Fig. 5 summarizes the ultimate tensile stress, break stress, and Young's modulus of the composites. Pure PLA had the highest tensile stress of 59.0 MPa and break stress of 53.1 MPa, with a Young's modulus of 2.8 GPa, which were comparable values with the results in Zhao *et al.*'s study.[5]

Compared to pure PLA composites, the introduction of untreated poplar into PLA composites slightly reduced tensile stress (49.8 MPa) and break stress (49.7 MPa), likely due to poor interfacial adhesion between hydrophilic biomass and the

Open Access Article. Published on 03 9 2025. Downloaded on 2026-04-26 3:20:06.
This article is licensed under a Creative Commons Attribution 3.0 Unported Licence.

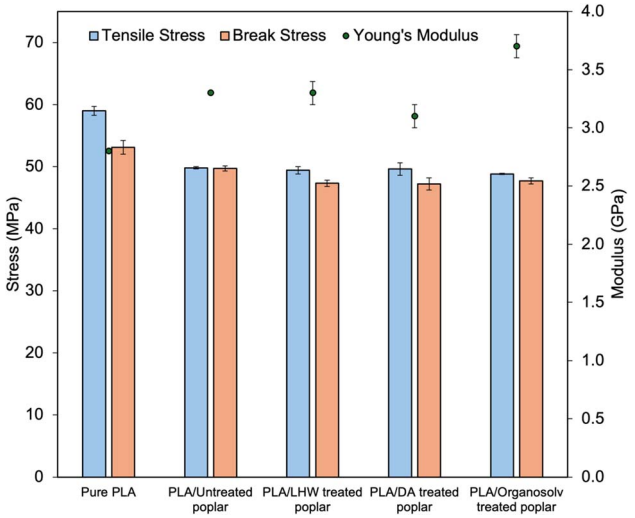

Fig. 5 Tensile results of pure PLA, PLA/untreated and treated poplar biocomposites.

hydrophobic PLA matrix. However, the composite stiffness increased significantly, with Young's modulus increasing to 3.3 GPa, mainly due to the high crystallinity and aspect ratio of cellulose enhancing the stiffness of biocomposites. The PLA/LHW and DA treated poplar composites showed further decreased tensile stress, 49.4 MPa for the PLA/LHW composite and 49.6 MPa for the PLA/DA one, and break stresses, 47.3 MPa for the PLA/LHW one and 47.2 MPa for the PLA/DA one, while maintaining a similar Young's modulus to the untreated biocomposites (PLA/LHW at 3.3 GPa and PLA/DA at 3.1 GPa). This suggests that although these pretreatments improved the hydrophobicity of poplar and reduced hemicellulose content, which could potentially aid dispersion,[41] these changes did not translate into improved load-bearing capacity. For instance, pseudo-lignin formed after DA pretreatment improved the hydrophobicity of poplar, but it may not have a strong interfacial bonding with structural biomass components like cellulose, leading to a reduction in tensile stress.

However, the PLA/organosolv treated poplar composite exhibited a significant increase in Young's modulus to 3.7 GPa (34% improvement compared to that of pure PLA composite) with comparable tensile (48.8 MPa) and break stress (47.7 MPa) to other composites. The enhanced stiffness could be attributed to synergistic factors: (i) higher cellulose content (78.8%), which increased the crystallinity of the PLA matrix as a nucleating agent; and (ii) a more rigid fiber structure due to the removal of amorphous components such as hemicellulose and lignin. These structural advantages allowed the PLA/organosolv treated poplar composite to resist deformation more effectively, thereby enhancing the modulus without compromising strength.

Overall, all biomass composites showed a higher Young's modulus than pure PLA composites, which indicated that the addition of biomass as a filler improved the stiffness of the biocomposite, which was also observed in the previous study.[16] However, no significant difference was found among PLA/poplar biocomposites in tensile stress and break stress, indicating that the effect of pretreatment was not significant on the tensile stress of the biocomposites. For Young's modulus, the PLA/organosolv treated poplar composites showed the highest modulus. This result was attributed to higher cellulose content because its crystalline structure provided stiffness to biocomposites. In the previous study, the cellulose fibers enhanced Young's modulus of biocomposites by providing a crystalline structure that resists deformation.[42] The high aspect ratio of cellulose fibers also allows for effective load transfer from the PLA matrix to the cellulose fibers, thereby improving the overall stiffness of the composite.[43] These previous observations align with the results in this study, suggesting that cellulose content in biomass significantly affected Young's modulus of the biocomposite.

Although the increased hydrophobicity of biomass through pretreatment could improve stress transfer between the particles and the matrix, the tensile stress and break stress were not improved. Thus, the tensile stress of PLA/poplar composites appeared to be dependent on the content of biomass in PLA rather than lignin modification.[16] Hence, the hydrophobicity of biomass was not as significant as we hypothesized in the determination of the mechanical performance of the 3D printed biomass reinforced PLA composites. Instead, organosolv treated biomass addition led to better stiffness of PLA/biomass biocomposites than those of LHW and DA treated biomass.

In summary, the pretreatments (LHW, DA, and organosolv) enhanced the surface properties of poplar (more hydrophobic and hemicellulose removal) but did not significantly improve tensile stress or break stress compared to PLA/untreated poplar composites. However, the Young's modulus of the PLA/organosolv treated composite was significantly increased (3.8 GPa), highlighting the potential of pretreatment to enhance stiffness through improved crystallinity and cellulose content. Notably, PLA/untreated poplar composites exhibited comparable mechanical properties and even slightly higher tensile and break stress than PLA/treated poplar composites. These findings indicated that untreated poplar also has promising potential as a filler in biocomposites without additional chemical modification, potentially reducing processing costs and simplifying production.

On the other hand, biomass pretreatment remains a valuable strategy for modifying filler characteristics. As demonstrated by organosolv treated biocomposites, tuning parameters such as cellulose content and morphological properties can enhance specific properties like stiffness (modulus). Therefore, by strategically altering biomass composition and structure, the performance of biocomposites can be further optimized for specific applications. Since the characteristics and behaviors of biocomposites can be tailored through pretreatment parameters such as severity, future studies focused on fine-tuning pretreatment conditions, fiber size, and filler loading will be essential to fully investigate the potential of PLA/biomass biocomposites across diverse applications.

To investigate the impact of cellulose on the mechanical properties of the biocomposites, cellulose DP of untreated and treated poplar was analyzed. Fig. 6 shows the weight-average degree of polymerization (DP_w) of cellulose, the number-

© 2025 The Author(s). Published by the Royal Society of Chemistry

Open Access Article. Published on 03 9 2025. Downloaded on 2026-04-26 3:20:06.
This article is licensed under a Creative Commons Attribution 3.0 Unported Licence.

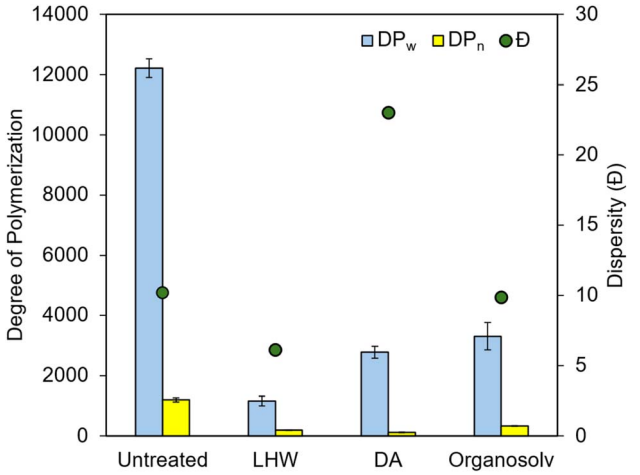

Fig. 6 Cellulose degree of polymerization and dispersity (*Đ*) of untreated and treated poplar.

average degree of polymerization (DP_n) of cellulose, and the dispersity (*Đ*). The cellulose in untreated poplar showed a DP_n of 1199 and DP_w of 12 213, resulting in a *Đ* of 10.20, which indicated a relatively broad molecular weight distribution. However, the chemical pretreatment significantly reduced these values: the cellulose in LHW treated poplar had a DP_n of 190, DP_w of 1164, and *Đ* of 6.13; the DA treated poplar showed a DP_n of 121, DP_w of 2778, and *Đ* of 23.03; and the organosolv treated one showed a DP_n of 336, a DP_w of 3311, and a *Đ* of 9.88. The difference in cellulose DP and dispersity between LHW and DA treatments can be attributed to both the chemical severity and reaction conditions of the two pretreatments.[44] LHW pretreatment was conducted at 200 °C for 20 minutes, selectively hydrolyzing hemicellulose while largely preserving cellulose.[45] This mild, non-acidic process resulted in moderate DP values and a relatively narrow *Đ*, indicating uniform chain lengths. In contrast, DA pretreatment was performed at a lower temperature of 160 °C but with 0.5 wt% H_2SO_4, which not only removed hemicellulose but also partially degraded cellulose,[46] leading to shorter cellulose chains and a broader molecular weight distribution. According to the results, there was no significant or direct correlation observed between cellulose DP and the mechanical properties of the PLA/poplar composites among the three different pretreatment methods. Although substantial changes in cellulose DP and dispersity in each pretreatment were observed, they were not involved in the enhancement of the mechanical properties of the biocomposites. However, it is worth noting that LHW and DA treated poplar showed similar chemical compositions but significantly different cellulose DP and *Đ* values. Despite DA treated poplar having a higher DP_w and much broader *Đ*, the mechanical performance of its composite was similar to that of PLA/LHW treated poplar composites. This comparison suggests that cellulose DP may influence composite properties, but its effect is secondary to other factors such as interfacial adhesion and filler dispersion.

3.2.2. Thermal properties of PLA/biomass biocomposites. To understand the impacts of each pretreatment on the thermal properties of the PLA/biomass composites like glass transition temperature (T_g), cold crystallization temperature (T_{cc}), melting temperature (T_m), and PLA crystallinity changes in the biocomposites, DSC was carried out by heat/cool/heat cycles. Table 2 and Fig. 7 show the thermal properties of pure PLA and PLA/poplar biocomposites. The glass transition temperature for pure PLA was reported at 61.0 °C, with no cold crystallization temperature observed, and a melting temperature of 150.9 °C. The degree of crystallinity (X_c) for pure PLA was the lowest at 1.9%. Similarly, Yang and Du reported that the T_g and T_m of pure PLA were 59.8 °C and 151.8 °C, respectively, with a T_{cc} present at 128.2 °C.[47] The PLA/untreated poplar composite showed a similar T_g at 60.7 °C, T_{cc} appearing at 125.2 °C and T_m closely matching with that of pure PLA at 150.2 °C. The X_c of the biocomposite was more than double that of pure PLA at 4.4%. Composites with LHW treated biomass exhibit a T_g of 60.4 °C, T_{cc} at 125.6 °C, and T_m of 150.3 °C, with an X_c of 5.0%. The PLA/DA treated poplar composites had T_g at 60.7 °C, with T_{cc} at 125.7 °C, T_m at 150.1 °C, and an X_c of 4.7%. Finally, the PLA/organosolv treated poplar composite displayed a T_g of 60.4 °C, T_{cc} of 124.9 °C, and T_m of 150.0 °C. It had the highest X_c among all the composites at 7.3%, indicating a significant increase in the ordered structure of PLA when organosolv treated poplar was used as a filler.[48]

Despite the similar T_g and T_m among the composites with untreated and treated poplar, the melting enthalpy and degree of crystallinity significantly increased by the addition of those poplar samples. In addition, the presence of a cold crystallization peak was observed with the addition of untreated and treated poplar. Cold crystallization occurs when crystallization happens during the heating process and above T_g due to the molecular chains regaining mobility, while below T_g, there will be a significant restriction.[49] This observation showed that the additional loading of biomass could increase the crystallinity of the 3D printed composites and suggested that the biomass fillers could act as nucleating agent inducing the crystallization

Table 2 Onset temperature (T_{onset}), glass transition temperature (T_g), cold crystallization temperature (T_{cc}), melting temperature (T_m), and degree of crystallinity (X_c) of pure PLA and PLA/untreated and treated poplar biocomposites from TGA and DSC

Sample	T_{onset} (°C)	T_g (°C)	T_{cc} (°C)	T_m (°C)	X_c (%)
Pure PLA	301.1	61.0	—	150.9	1.9
PLA/untreated poplar	290.2	60.7	125.2	150.2	4.4
PLA/LHW treated poplar	296.4	60.4	125.6	150.3	5.0
PLA/DA treated poplar	294.7	60.7	125.7	150.1	4.7
PLA/organosolv treated poplar	291.1	60.4	124.9	150.0	7.3

Open Access Article. Published on 03 9 2025. Downloaded on 2026-04-26 3:20:06.
This article is licensed under a Creative Commons Attribution 3.0 Unported Licence.

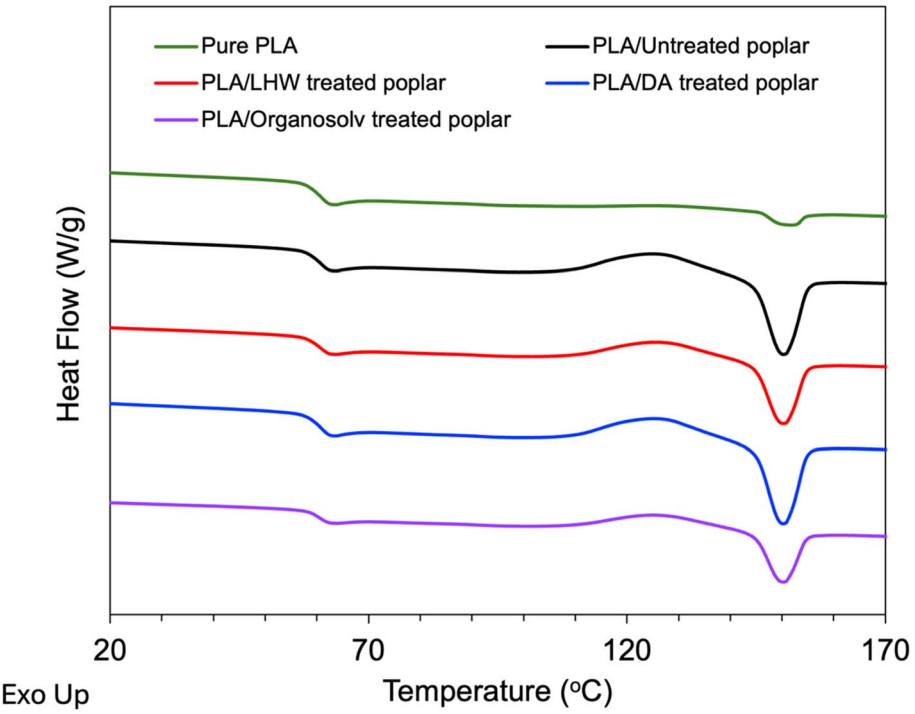

Fig. 7 DSC curve of pure PLA and PLA/untreated and treated poplar biocomposites.

of PLA. Similar to traditional petroleum-based nucleating agents, with the addition of small molecular biomass into the PLA matrix, the biomass molecules could be dispersed in the matrix and increase the crystallization sites of PLA and nucleation density. As a result, the nucleation of PLA can occur at the site of small-molecule biomass, thereby shortening nucleation time. Consequently, this leads to an accelerated crystallization rate and increases the crystallinity of PLA.[50] A simliar observation was also in Silva *et al.*'s study. They investigated the non-isothermal cold crystallization behavior of pure PLA and cork–polymer composites (CPC) using DSC at different heating rates. The results showed that T_{cc} significantly decreased with the addition of cork, and the authors concluded that cork can act as a nucleating agent during the non-isothermal cold crystallization process by increasing the crystallization rate of the PLA matrix.[51]

To study the effects of thermochemical pretreatments on the thermal properties of biomass and biocomposites, TGA was carried out. One onset temperature (T_{onset}) was observed from TGA chromatography. The TGA results provide the thermal stability of untreated and treated poplar samples (Fig. 8). The thermal degradation temperatures for untreated, LHW, DA, and organosolv treated poplar were 303.1 °C, 331.6 °C, 325.4 °C, and 322.8 °C, respectively. Untreated poplar showed a typical thermal degradation onset for lignocellulosic biomass due to the combined effects of cellulose, hemicellulose, and lignin. Among the treated samples, LHW treated poplar exhibited the highest thermal degradation onset temperature, indicating improved thermal stability, possibly due to the effective removal of hemicellulose, resulting in a residue with higher cellulose and lignin contents. Similarly, DA treated poplar and organosolv treated poplar had enhanced thermal stability compared to the untreated sample, which was due to the effective removal of hemicellulose, leading to a higher cellulose content.[52] Although LHW and DA pretreatments resulted in similar chemical compositions, their thermal degradation behaviors were different. LHW treated poplar had a slightly higher onset temperature but lower residual mass compared to DA treated poplar, which is likely due to differences in the structural and chemical modifications induced by the two pretreatments. LHW pretreatment primarily hydrolyzed hemicellulose and partially solubilized low-molecular-weight fractions, producing a more thermally stable residue rich in cellulose and lignin. In contrast, DA pretreatment led to the formation of pseudo-lignin – a thermally stable, carbon-rich substance that is generated through acid-catalyzed dehydration of carbohydrates to furfural and 5-hydroxymethylfurfural (5-HMF) followed by their condensation and polymerization into aromatic structures.[35,53] Pseudo-lignin was deposited on the fiber surface and contributes to the higher residual mass observed in DA treated samples, while potentially interfering with the overall thermal decomposition pathway. Overall, the TGA results indicated that pretreatment methods significantly impacted the thermal stability of poplar biomass, with LHW treatment providing the highest stability, followed by DA and organosolv treatments. These findings are essential for understanding how pretreatments affect the thermal properties of the biomass, which in turn impacts the performance of the resulting biocomposites.

These differences in the thermal stability of untreated and treated biomass were also reflected in the thermal behavior of the corresponding 3D printed biocomposites. As shown in

© 2025 The Author(s). Published by the Royal Society of Chemistry

Open Access Article. Published on 03 9 2025. Downloaded on 2026-04-26 3:20:06.
This article is licensed under a Creative Commons Attribution 3.0 Unported Licence.

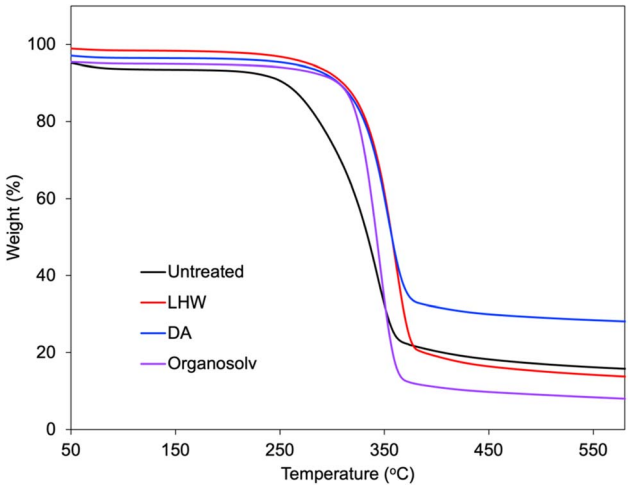

Fig. 8 TGA curve of untreated and treated poplar.

Table 2, pure PLA exhibits the highest decomposition onset temperature at 301.1 °C, suggesting good thermal stability. The addition of untreated poplar decreases the decomposition onset temperature of the composite to 290.2 °C, indicating that the incorporation of poplar affected the thermal performance of composites. The PLA/LHW treated poplar composites demonstrate a slightly higher T_{onset} of 296.4 °C compared to other chemical pretreatments. The DA pretreatment resulted in a T_{onset} of 294.7 °C, while the PLA/organosolv treated poplar composite displays the lowest decomposition onset temperature at 291.1 °C among the chemical pretreatments. As a result, with the addition of untreated and treated poplar, the decomposition temperature of composites was decreased compared to that of pure PLA which was mainly due to the low decomposition temperature of poplar. However, with the highest xylan and lignin removals, the PLA/organosolv treated poplar composite had the lowest decomposition temperature, while the PLA/LHW treated poplar composite having more lignin content showed the highest decomposition temperature among the PLA/treated poplar composites. This observation suggested that the chemical composition in the biomass can greatly impact the thermal stability of polymer composites due to lignin having higher decomposition temperatures compared to hemicellulose and cellulose.[54] Additionally, it is important to acknowledge that the varying molecular weights of biomass components also contribute to differences in their respective decomposition temperatures.[55]

3.2.3. Morphological properties of PLA/biomass composites. Fig. 9 shows the fracture surface of the 3D printed sample after tensile testing at 1000× magnification. No significant defects or voids were observed between the PLA matrix and biomass particles, which indicated no major discontinuities at the micro scale. No significant difference was observed among PLA/poplar biocomposites, which indicated that the chemical modification did not significantly improve the compatibility of the biocomposites. However, some fibers (indicated by arrows) were observed from PLA/organosolv treated poplar biocomposites (Fig. 9e), which could mainly be attributed to its cellulose fraction.[56] These cellulose fibers could be the main component that significantly improved the stiffness of the biocomposites compared to others.[57] Hence, the morphological properties of PLA/poplar biocomposites also suggested that cellulose would be the main component that affects the mechanical properties of the composite materials.

3.3. Correlations between biomass properties and biocomposite performance

To assess the relationships between properties of poplar and technical performance of PLA/poplar biocomposites, PCA was

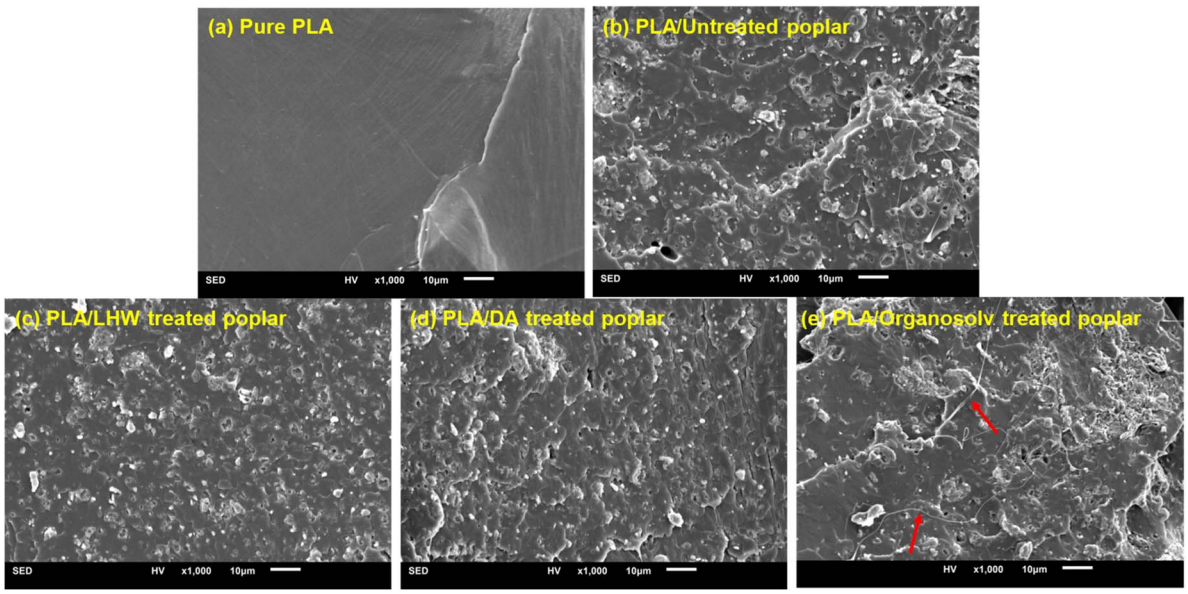

Fig. 9 SEM images of the cross-section of the 3D printed sample after tensile testing: (a) the pure PLA composite and PLA/poplar biocomposites with (b) untreated, (c) LHW, (d) DA and (e) organosolv treated poplar.

Open Access Article. Published on 03 9 2025. Downloaded on 2026-04-26 3:20:06. This article is licensed under a Creative Commons Attribution 3.0 Unported Licence.

conducted with experimental data obtained in this study including chemical composition (glucan, xylan, and lignin), particle size, SSA, cellulose DPs and $Đ$, and WCA of untreated and treated poplar as well as tensile properties (tensile stress, break stress, and modulus), decomposition temperature, and X_c of biocomposites. For ease of comparison across pretreatment methods, a summary of key parameters is provided in the SI (Table S1). Fig. 10 shows that 90.72% of the total variation (the sum of PC1 and PC2) is explained by the first two principal components, suggesting a close interrelation between the chemical composition and physicochemical properties of poplar and the mechanical and thermal performance of biocomposites. The direction and length of each arrow reflect how strongly each variable contributes to the principal components, allowing a visual assessment of their relationships.

First, the SSA and WCA, representing the surface characteristics of the biomass, were shown to have a relationship with the thermal decomposition behavior of the composites. SSA represents the total surface area per unit mass of the material. In biomass, higher SSA means a larger surface area, which could impact the rate of thermal degradation.[58] High SSA also led to extensive interfacial interactions between the biomass and the polymer matrix, enhancing the thermal stability of biocomposites by promoting better stress distribution and heat dissipation throughout the material.[59,60] Additionally, the particle size of biomass was found to have a negative correlation with SSA, suggesting that finer particles with higher surface area enhance interfacial adhesion, thereby improving composite thermal stability. WCA also affected the interactions between the biomass particles and the polymer matrix during the thermal decomposition process. For example, if the biomass is hydrophilic (low WCA), it may not bond well with hydrophobic polymers, which could lead to degradation at lower temperatures. On the other hand, if the biomass is hydrophobic (high WCA), it can interact more strongly with the polymer matrix, potentially improving the thermal stability of the biocomposite. Hence, the WCA affects the interfacial bonding between biomass and the polymer matrix, further impacting the thermal stability.[61,62] In our study, DA treated poplar exhibited the highest WCA (76 ± 3°), and the corresponding composites showed higher onset degradation temperature (294.7 °C) than the untreated one (290.2 °C), indicating enhanced interfacial compatibility and thermal resistance. However, the lignin content of biomass was oriented in the same direction as the decomposition temperature of biocomposites but in the opposite direction from the modulus of biocomposites, implying a positive correlation with thermal stability but a negative correlation with stiffness. Although lignin is thermally stable, its complex and amorphous structure may interfere with PLA crystallization and interfacial compatibility, potentially reducing the rigidity of the biocomposites.[63]

For mechanical properties, the cellulose DPs and xylan content in the biomass appear to be correlated with the break stress of the biocomposites. Longer cellulose chains (high DP) are generally associated with improved mechanical properties due to their capacity to entangle more effectively, hence distributing applied stress more evenly. Thus, biocomposites with a higher cellulose DP in the biomass can have a better ability to sustain load up to the point of fracture.[64,65] For instance, the PLA/untreated poplar composites contained cellulose with the highest DP (DP_n of 1199 and DP_w of 12 213), exhibited higher break stress compared to the PLA/treated biomass composites, further supporting the correlation between the cellulose chain length and stress-bearing capacity. Moreover, xylan, as an amorphous polysaccharide, can impact the properties of biocomposites differently. The removal of xylan may enhance the dispersion of cellulose fibers, thus improving the uniformity and tensile stress of the composites. However, in some cases, small amounts of amorphous xylan can act as "glue" to facilitate better stress transfer between the biomass filler and the polymer matrix by improving compatibility or adhesion at the interface, which could positively impact the break stress.[66,67] In our study, the PLA/untreated poplar composite with relatively high xylan content in untreated poplar demonstrated break stress values (49.7 MPa) similar to those of treated samples, suggesting that retained xylan may contribute positively to stress transfer in some cases.

Finally, the PCA result showed that the modulus of biocomposites was closely related to the degree of crystallinity, while the glucan content is positioned in a similar direction as X_c, indicating a positive correlation. This suggests that higher glucan content in biomass contributes to increased crystallinity in the composite, since most glucan in biomass is from cellulose. As the X_c of biocomposites increases, so does the stiffness, leading to a higher Young's modulus. This enhancement of stiffness suggested that the biomass fillers can act as nucleating agents to promote the crystallization of PLA, thereby improving the rigidity of the biocomposite material.[68,69] For example, the organosolv treated biocomposite showed the highest crystallinity (X_c = 7.3%) and also exhibited the highest Young's modulus (3.7 GPa), clearly demonstrating this relationship. In contrast, cellulose dispersity of biomass was oriented in the opposite direction from both X_c and modulus of biocomposites in the PCA plot, implying a negative correlation. This indicates that broader molecular weight distributions may hinder the

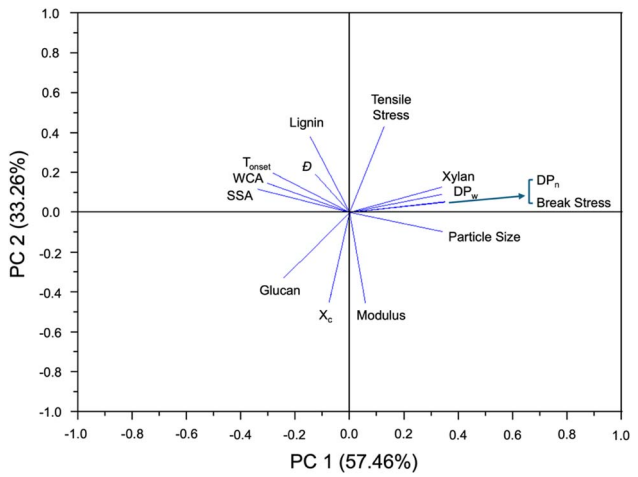

Fig. 10 Biplots of the first principal component (PC1) and second principal component (PC2) from a PCA analysis.

© 2025 The Author(s). Published by the Royal Society of Chemistry

Open Access Article. Published on 03 9 2025. Downloaded on 2026-04-26 3:20:06.
This article is licensed under a Creative Commons Attribution 3.0 Unported Licence.

uniform chain packing and reduce the efficiency of PLA crystallization. As a result, higher cellulose dispersity could compromise the stiffness of the resulting biocomposites, further emphasizing the importance of uniform cellulose chain length in optimizing mechanical properties. For example, although DA treated poplar and LHW treated poplar had similar chemical composition, the DA treated biomass exhibited a much higher cellulose dispersity ($Đ = 23.03$) compared to LHW treated biomass ($Đ = 6.13$). This broader molecular weight distribution in DA treated cellulose is consistent with a lower Young's modulus (3.1 GPa) in the corresponding composite compared to the LHW treated one (3.3 GPa), suggesting that high cellulose dispersity may limit stiffness enhancement despite comparable cellulose content.

4 Conclusion

This study investigated the effects of the characteristics of the biomass filler on 3D printed PLA/biomass biocomposite materials with differently processed poplar *via* LHW, DA, and organosolv pretreatments. Several physicochemical, thermal, and morphological properties, as well as the chemical composition of biomass, were transformed by each pretreatment. The processed poplar biomass fillers induced crystallization and improved the stiffness of the biocomposites. The Young's modulus of the 3D printed PLA/organosolv treated poplar was 34% higher than that of the pure PLA composite, while the tensile stress and break stress of PLA/organosolv treated poplar were not improved. The results indicated that cellulose content in the biomass was the main influencing factor in determining the stiffness of the composite. PCA results revealed multiple key relationships between biomass characteristics and biocomposite performance. Cellulose DPs and xylan content in the biomass were correlated with the break stress of the composites, while glucan content in biomass showed a positive correlation with crystallinity of biocomposites, which aligned with increased modulus. Conversely, cellulose dispersity was negatively correlated with both crystallinity and stiffness of composites, suggesting that broader molecular weight distributions may hinder effective crystallization and reduce rigidity. SSA and WCA, representing surface characteristics, were positively correlated with decomposition temperature, highlighting the role of interfacial properties in thermal stability. Lignin content appeared to negatively correlate with the composite modulus, likely due to its amorphous structure interfering with PLA crystallization. These findings demonstrate three important outcomes: first, biomass pretreatment is a valuable strategy for tuning biofiller properties. As observed with organosolv treated poplar composites, adjusting parameters such as cellulose content and surface characteristics can selectively enhance specific performance like stiffness. Second, strategic modification of biomass composition enables tailored optimization of PLA/biomass composites for targeted applications. Third, a particle size reduction approach, like ball-milling, potentially makes biomass a reinforcing filler in composites without chemical treatment, simplifying the manufacturing process and reducing additional processing steps in biocomposite production. Together, these insights will be beneficial for guiding future biocomposite process development and material design. The current understanding of the relationships between biomass properties and composite performance can be used to design the targeted biomass processing approach based on the required properties and performance. Furthermore, additional modifications of biomass feedstock can be made based on the findings of this study to enhance the biocomposite properties.

Author contributions

Anqi Ji: conceptualization, data curation, formal analysis, investigation, methodology, writing – original draft, writing – review & editing. Samarthya Bhagia: formal analysis, data curation, investigation, methodology, writing – review & editing. Nara Han: formal analysis, investigation. Kwang Ho Kim: investigation, methodology. Gyu Leem: investigation. Nidia C. Gallego: formal analysis. Shuyang Zhang: formal analysis, investigation, writing – review & editing. Kai Li: formal analysis, writing – review & editing. Soydan Ozcan: formal analysis. Arthur J. Ragauskas: conceptualization, supervision, project administration, resources, writing – review & editing. Chang Geun Yoo: conceptualization, methodology, supervision, project administration, resources, writing – original draft, writing – review & editing.

Conflicts of interest

The authors declare no conflict of interest.

Data availability

The data supporting this article have been included as part of the SI. See DOI: **https://doi.org/10.1039/d5su00327j**.

Acknowledgements

This study was supported by the Global Center for Sustainable Bioproducts with the National Science Foundation Office of International Science and Engineering (NSF OISE 2435227). This work was also funded, in part, by the Laboratory Directed Research and Development Program of Oak Ridge National Laboratory, managed by UT-Battelle, LLC, for the U.S. Department of Energy under Contract DE-AC05-00OR22725. The United States Government retains and the publisher, by accepting the article for publication, acknowledges that the United States Government retains a nonexclusive, paid-up, irrevocable, worldwide license to publish or reproduce the published form of this manuscript, or allow others to do so, for United States Government purposes. The Department of Energy will provide public access to these results of federally sponsored research in accordance with the DOE Public Access Plan (**https://energy.gov/downloads/doe-public-access-plan**). The views and opinions of the authors expressed herein do not necessarily state or reflect those of the United States Government or any agency thereof. Neither the United States

Open Access Article. Published on 03 9 2025. Downloaded on 2026-04-26 3:20:06.
This article is licensed under a Creative Commons Attribution 3.0 Unported Licence.

Government nor any agency thereof, nor any of their employees, makes any warranty, expressed or implied, or assumes any legal liability or responsibility for the accuracy, completeness, or usefulness of any information, apparatus, product, or process disclosed, or represents that its use would not infringe privately owned rights.

References

1 H. N. Chia and B. M. Wu, *J. Biol. Eng.*, 2015, **9**, 1–14.
2 B. Brenken, E. Barocio, A. Favaloro, V. Kunc and R. B. Pipes, *Addit. Manuf.*, 2018, **21**, 1–16.
3 T. D. Ngo, A. Kashani, G. Imbalzano, K. T. Nguyen and D. Hui, *Composites, Part B*, 2018, **143**, 172–196.
4 J. Yang, X. An, L. Liu, S. Tang, H. Cao, Q. Xu and H. Liu, *Carbohydr. Polym.*, 2020, 116881.
5 X. Zhao, H. Tekinalp, X. Meng, D. Ker, B. Benson, Y. Pu, A. J. Ragauskas, Y. Wang, K. Li and E. Webb, *ACS Appl. Bio Mater.*, 2019, **2**, 4557–4570.
6 N. Ayrilmis, M. Kariz, J. H. Kwon and M. Kitek Kuzman, *Int. J. Adv. Manuf. Technol.*, 2019, **102**, 2195–2200.
7 M. S. Oh, H. Y. Yoon, N. T. Phong, Y. Lee, K. H. Kang, Y. M. Kim, K. S. Kim and J.-R. Jeon, *Environ. Technol. Innovation*, 2024, **36**, 103794.
8 S. P. Antai and D. L. Crawford, *Appl. Environ. Microbiol.*, 1981, **42**, 378–380.
9 Y. Tao, H. Wang, Z. Li, P. Li and S. Q. Shi, *Materials*, 2017, **10**, 339.
10 J. Liu, L. Sun, W. Xu, Q. Wang, S. Yu and J. Sun, *Carbohydr. Polym.*, 2019, **207**, 297–316.
11 C. E. Wyman, B. E. Dale, R. T. Elander, M. Holtzapple, M. R. Ladisch, Y. Lee, C. Mitchinson and J. N. Saddler, *Biotechnol. Prog.*, 2009, **25**, 333–339.
12 V. A. Thomas, B. S. Donohoe, M. Li, Y. Pu, A. J. Ragauskas, R. Kumar, T. Y. Nguyen, C. M. Cai and C. E. Wyman, *Biotechnol. Biofuels*, 2017, **10**, 1–13.
13 X. Pan, D. Xie, R. W. Yu, D. Lam and J. N. Saddler, *Ind. Eng. Chem. Res.*, 2007, **46**, 2609–2617.
14 V. Raghavendran, C. Nitsos, L. Matsakas, U. Rova, P. Christakopoulos and L. Olsson, *AMB Express*, 2018, **8**, 1–8.
15 ASTM International, *Standard Test Method for Tensile Properties of Plastics*, ASTM D638-22, 2022, DOI: **10.1520/D0638-22**.
16 S. Bhagia, R. R. Lowden, D. Erdman III, M. Rodriguez Jr, B. A. Haga, I. R. M. Solano, N. C. Gallego, Y. Pu, W. Muchero and V. Kunc, *Appl. Mater. Today*, 2020, **21**, 100832.
17 A. Sluiter, B. Hames, R. Ruiz, C. Scarlata, J. Sluiter, D. Templeton and D. Crocker, *Laboratory Analytical Procedure: Determination of Structural Carbohydrates and Lignin in Biomass*, 2008, pp. 1–16.
18 X. Meng, Y. Pu, C. G. Yoo, M. Li, G. Bali, D.-Y. Park, E. Gjersing, M. F. Davis, W. Muchero and G. A. Tuskan, *ChemSusChem*, 2016, **10**, 139–150.
19 ASTM International, *Standard Test Method for Thermal Stability by Thermogravimetry*, ASTM E2550-21, 2021, DOI: **10.1520/E2550-21**.
20 Y. Liu, S. Jiang, W. Yan, M. He, J. Qin, S. Qin and J. Yu, *Polymers*, 2020, **12**, 1563.
21 Z.-M. Zhao, X. Meng, B. Scheidemantle, Y. Pu, Z.-H. Liu, B.-Z. Li, C. E. Wyman, C. M. Cai and A. J. Ragauskas, *Bioresour. Technol.*, 2022, **347**, 126367.
22 R. Sepe, F. Bollino, L. Boccarusso and F. Caputo, *Composites, Part B*, 2018, **133**, 210–217.
23 X. Ma, X. Yang, X. Zheng, L. Chen, L. Huang, S. Cao and H. Akinosho, *Cellulose*, 2015, **22**, 1687–1696.
24 P. Sannigrahi, D. H. Kim, S. Jung and A. Ragauskas, *Energy Environ. Sci.*, 2011, **4**, 1306–1310.
25 C. Liu and C. E. Wyman, *Bioresour. Technol.*, 2005, **96**, 1978–1985.
26 H. Jaya, M. F. Omar, H. M. Akil, Z. A. Ahmad and N. N. Zulkepli, *BioResources*, 2016, **11**, 6489–6504.
27 A. Y. Al-Maharma, S. P. Patil and B. Markert, *Mater. Res. Express*, 2020, 122001.
28 H. Yang, Z. Shi, G. Xu, Y. Qin, J. Deng and J. Yang, *Bioresour. Technol.*, 2019, **274**, 261–266.
29 M. Kapoor, T. Raj, M. Vijayaraj, A. Chopra, R. P. Gupta, D. K. Tuli and R. Kumar, *Carbohydr. Polym.*, 2015, **124**, 265–273.
30 W. Wang, X. Chen, B. S. Donohoe, P. N. Ciesielski, R. Katahira, E. M. Kuhn, K. Kafle, C. M. Lee, S. Park and S. H. Kim, *Biotechnol. Biofuels*, 2014, **7**, 1–13.
31 J. Jiang, J. Wang, X. Zhang and M. Wolcott, *Ind. Crops Prod.*, 2017, **97**, 498–508.
32 T. Fujita, D. Nakagawa, K. Komiya, S. Ohira and I. Hanasaki, *Nanomaterials*, 2022, **12**, 2431.
33 M. F. Hossain, S. N. Shuvo and M. Islam, *Procedia Eng.*, 2014, **90**, 46–51.
34 E. Rojo, M. S. Peresin, W. W. Sampson, I. C. Hoeger, J. Vartiainen, J. Laine and O. J. Rojas, *Green Chem.*, 2015, **17**, 1853–1866.
35 S. D. Shinde, X. Meng, R. Kumar and A. J. Ragauskas, *Green Chem.*, 2018, **20**, 2192–2205.
36 F. Hu, S. Jung and A. Ragauskas, *ACS Sustainable Chem. Eng.*, 2013, **1**, 62–65.
37 R. Kumar, F. Hu, P. Sannigrahi, S. Jung, A. J. Ragauskas and C. E. Wyman, *Biotechnol. Bioeng.*, 2013, **110**, 737–753.
38 J. Zhuang, M. Li, Y. Pu, A. J. Ragauskas and C. G. Yoo, *Appl. Sci.*, 2020, **10**, 4345.
39 J. Zhu, H. Sun, B. Yang and Y. Weng, *Materials*, 2024, **17**, 336.
40 E. Vengadesan, S. Morakul, S. Muralidharan, P. K. Pullela, A. Alarifi and T. Arunkumar, *Discover Appl. Sci.*, 2025, **7**, 161.
41 D. K. Giang, S.-E. Ban, J.-H. Choi, H. Seong, C.-D. Jung, H. Kim and J.-W. Lee, *Int. J. Biol. Macromol.*, 2022, **215**, 36–44.
42 A. Riley, in *Packaging Technology*, Elsevier, 2012, pp. 262–286.
43 K. Keeratipinit, P. Wijaranakul, W. Wanmolee and B. Hararak, *ACS Omega*, 2024, **9**, 26159–26167.
44 M. Li, S. Cao, X. Meng, M. Studer, C. E. Wyman, A. J. Ragauskas and Y. Pu, *Biotechnol. Biofuels*, 2017, **10**, 1–13.
45 A. K. Kumar and S. Sharma, *Bioresources and Bioprocessing*, 2017, **4**, 7.
46 P. Kumar, D. M. Barrett, M. J. Delwiche and P. Stroeve, *Ind. Eng. Chem. Res.*, 2009, **48**, 3713–3729.

© 2025 The Author(s). Published by the Royal Society of Chemistry

Open Access Article. Published on 03 9 2025. Downloaded on 2026-04-26 3:20:06.
This article is licensed under a Creative Commons Attribution 3.0 Unported Licence.

47 H. Yang and J. Du, *Molecules*, 2023, **29**, 169.
48 K. Dome, E. Podgorbunskikh, A. Bychkov and O. Lomovsky, *Polymers*, 2020, **12**, 641.
49 A. Ji, S. Zhang, S. Bhagia, C. G. Yoo and A. J. Ragauskas, *RSC Adv.*, 2020, **10**, 21698–21723.
50 K. Shi, G. Liu, H. Sun, B. Yang and Y. Weng, *Polymers*, 2022, **14**, 4305.
51 S. Magalhaes da Silva, M. A. Silva and J. M. Oliveira, *J. Therm. Anal. Calorim.*, 2021, **146**, 1667–1678.
52 F. Shi, Y. Wang, M. Davaritouchaee, Y. Yao and K. Kang, *ACS Omega*, 2020, **5**, 24780–24789.
53 N. Chen, K. Jiang, M. Zhao, C. Zhang, Y. Jin and W. Wu, *Biomass Bioenergy*, 2024, **188**, 107339.
54 S. A. El-Sayed, T. M. Khass and M. E. Mostafa, *Biomass Convers. Biorefin.*, 2023, 1–25.
55 A. Olszewski, P. Kosmela, L. Vēvere, M. Kirpluks, U. Cabulis and Ł. Piszczyk, *Sci. Rep.*, 2024, **14**, 812.
56 Q. Wang, J. Zhu, R. Gleisner, T. Kuster, U. Baxa and S. McNeil, *Cellulose*, 2012, **19**, 1631–1643.
57 G. Josefsson, F. Berthold and E. K. Gamstedt, *Int. J. Solids Struct.*, 2014, **51**, 945–953.
58 M. Kurgankina, G. Nyashina, A. Shvets, K. Vershinina and A. O. Pereira Junior, *Appl. Sci.*, 2022, **12**, 12442.
59 A. Codou, M. Misra and A. K. Mohanty, *Composites, Part A*, 2018, **112**, 1–10.
60 B. P. Chang, A. Rodriguez-Uribe, A. K. Mohanty and M. Misra, *Renewable Sustainable Energy Rev.*, 2021, **152**, 111666.
61 A. Orue, A. Jauregi, C. Peña-Rodriguez, J. Labidi, A. Eceiza and A. Arbelaiz, *Composites, Part B*, 2015, **73**, 132–138.
62 S. Qian, Y. Kong, H. Cheng, S. Tu and C. Zhai, *Surf. Interfaces*, 2023, **42**, 103315.
63 S. Frasca, C. S. Katsiotis, Å. Henrik-Klemens, A. Larsson, M. Strømme, J. Lindh, M. V. Galkin and J. Gising, *ACS Appl. Polym. Mater.*, 2024, **6**, 13574–13584.
64 A. Peterson, A. Y. Mehandzhiyski, L. Svenningsson, A. Ziolkowska, R. Kádár, A. Lund, L. Sandblad, L. Evenas, G. Lo Re and I. Zozoulenko, *Macromolecules*, 2021, **54**, 3507–3516.
65 S. Tanpichai, A. Boonmahitthisud, N. Soykeabkaew and L. Ongthip, *Carbohydr. Polym.*, 2022, **286**, 119192.
66 A. Pizzi, A. N. Papadopoulos and F. Policardi, *Polymers*, 2020, **12**, 1115.
67 X. Chen, X. Xi, A. Pizzi, E. Fredon, G. Du, C. Gerardin and S. Amirou, *J. Adhes.*, 2021, **97**, 873–890.
68 M. Hassan, A. K. Mohanty and M. Misra, *Mater. Des.*, 2023, 112558.
69 M. A. Morales, C. L. Atencio Martinez, A. Maranon, C. Hernandez, V. Michaud and A. Porras, *Polymers*, 2021, **13**, 1067.